Appl. Phys. A
DOI 10.1007/s00339-015-9213-1

Applied Physics A
Materials Science & Processing

Highly oxidized graphene nanosheets via the oxidization of detonation carbon

A. Nepal[1] · G. Chiu[1] · J. Xie[2] · G. P. Singh[3] · N. Ploscariu[1] · S. Klankowski[4] · T. Sung[1] · J. Li[4] · B. N. Flanders[1] · K. L. Hohn[2] · C. M. Sorensen[1]

Received: 4 February 2015 / Accepted: 3 May 2015

Abstract A unique approach was developed to produce highly oxygenated graphene nanosheets (OGNs) by solution-based oxidation of the pristine graphene nanosheets (GNs) prepared via a controlled detonation of acetylene with oxygen. The produced OGNs are about 250 nm in size and are hydrophilic in nature. The C/O ratio was dramatically reduced from 49:1 in the pristine GNs to about 1:1 in OGNs, as determined by X-ray photoelectron spectroscopy. This C/O in OGNs is the least ever found in all oxidized graphitic materials that have been reported. Thus, the OGNs produced from the detonated GNs with such high degree of oxidation herein yield a novel and promising material for future applications.

1 Introduction

Already considered one of the most pivotal materials of this century, single-layer graphene (SLG) is a one-atom-thick sheet of sp^2-bonded carbon atoms packed in honeycomb crystal lattice. It possesses superior physical properties like excellent electrical and thermal conductivity, optical transparency and mechanical strength [1–6]. New research is looking to employ these properties in areas such as nanoelectronics [7, 8], sensors [9], nanocomposite [10, 11], batteries [12], supercapacitors and hydrogen storage [13]. However, the complete exploitation of the proposed properties of SLG via promising applications has been a challenge since current large-scale production methods are not simple and economical. The largest issue lies in the irreversible agglomeration and restacking of graphene sheets via π–π interactions and van der Waals forces, forming multilayer graphite if sheet separation is not maintained [14, 15].

Processable graphene, chemically functionalized or surface-modified graphene which can be well dispersed in solvents, is thought as a remedy to this problem. Chemically functionalized graphene can be easily processed by solvent-assisted techniques like spin coating, layer-by-layer assembly and filtration. A suitable chemical functional group attached on the graphene sheet can prevent the agglomeration of single-layer graphene during its reduction in the solvent phase helping to maintain the inherent properties of SLG [16]. Graphite oxide prepared by oxidization of natural graphite has often been used as a starting material to prepare processable graphene. Graphite oxide contains highly oxygenated and hydrophilic layers which can be readily exfoliated in water to yield stable dispersions consisting mostly of single-layer sheets, i.e., graphene oxide [10, 17–20]. This dispersion capability facilitates a very feasible setting to carry out solution-phase techniques used to convert the graphene oxide back to graphene by chemical reduction [14, 18] and processing graphene oxides into films and paper-like materials [18, 19, 21–23]. Therefore, the preparation of aqueous dispersion of graphene oxide is

Electronic supplementary material The online version of this article (doi:10.1007/s00339-015-9213-1) contains supplementary material, which is available to authorized users.

✉ C. M. Sorensen
sor@phys.ksu.edu

[1] Department of Physics, Kansas State University, Manhattan, KS 66506, USA

[2] Department of Chemical Engineering, Kansas State University, Manhattan, KS 66506, USA

[3] Centre for Nanotechnology, Central University of Jharkhand, Ranchi 835205, Jharkhand, India

[4] Department of Chemistry, Kansas State University, Manhattan, KS 66506, USA

Published online: 10 May 2015

an important first step for the further applications of graphene by solution-phase surface manipulation.

Recently, we have demonstrated a unique method to produce the powder form of pristine graphene nanosheets (GNs) by a controlled detonation of acetylene (C_2H_2) with oxygen (O_2) [24]. This method is attractive due to the low cost and scalability. However, the GNs prepared by this new route are hydrophobic in nature and are not easy to be mixed with other chemicals and binders. This is a current challenge seen throughout the field of application of pristine GNs. Current research has shown that the application of pristine graphene in field effect transistors is not effective due to the absence of a band gap [25]. Hence, in order to further explore the landscape of the potential applications, functionalization of detonation-produced pristine GNs is needed.

Here we report on the formation of highly oxidized graphene nanosheets (OGNs) by oxidizing the pristine GNs prepared via a controlled detonation of acetylene with oxygen using a unique wet chemical approach which changed the C/O ratio of GNs from 49:1 to 1:1 for OGNs. Further, the OGNs dispersed in water were stable for several months.

2 Experimental procedures

2.1 Preparation of GNs

Powder GNs were prepared from the catalyst-free, controlled detonation of C_2H_2 gas in the presence of O_2 in a 16.6 l cylindrical aluminum chamber. For this study, GNs were prepared from a detonation with the pre-detonation molar ratio of $O_2/C_2H_2 = 0.8$. For each detonation, the initial chamber pressure was 1 atmosphere. The gases had purities of 98.0 % for C_2H_2 and 99.0 % for O_2. The detonation of C_2H_2 with O_2 was carried out by a controlled power supply through a spark generator ignition system. The GN formed under a typical peak detonation condition of temperature $\sim$4000 K and a peak pressure of 13.5 atmospheres. They were collected from the chamber approximately 10 min after detonation. For a detailed explanation of the experimental setup and mechanism of formation of GNs, refer to [24].

2.2 Preparation of OGNs from GNs

The pristine GNs produced by the detonation technique described above were oxidized by using a method designed for an improved oxidization of graphite flakes as described in the literature [26]. In this work, a typical 9/1 ratio of concentrated H_2SO_4/H_3PO_4 (270:30 ml) was added into a mixture 2 g of GNs and 6 g of $KMnO_4$ and the mixture was stirred overnight at a temperature $\sim$50 °C. The mixture was then cooled to room temperature and then the suspension was diluted with water (300 ml) and 30 % H_2O_2 (5 ml) in ice bath. The mixture was then centrifuged (7000 rpm for 30 min), and the supernatant was decanted away. The thick sludge at the bottom of the vial was diluted with water and again centrifuged. This intensive washing was repeated for about 7–10 times to remove any dissolved impurities. The sludge was then dried at room temperature, known as oxygenated graphene nanosheets (OGNs). During oxidation, no distinct color change was observed unlike the production of graphite oxides from the oxidation of graphite (which becomes bright yellow after diluting with H_2O_2). Instead, the suspension was dark black from start to end of the process. This might be because of the very small size ($\sim$250 nm) of the starting material, GNs.

3 Characterizations

X-ray diffraction was carried out using a Bruker D8 Advance X-ray diffractometer, Germany, with nickel filter Cu Kα radiation as the X-ray source to determine phase purity and degree of crystallization. Thermogravimetric analysis (TGA) of GNs and OGNs was carried out with a Perkin-Elmer Pyris1 TGA (Norwalk, CT) to determine the decomposition characteristics of the samples. About 5 mg of each sample was placed in the pan and heated from 50 to 600 °C at a heating rate of 20 °C/min under a nitrogen atmosphere. The layer and the size of the powder graphene samples were determined with a Philips CM-100 transmission electron microscope (TEM) with an accelerating voltage of 100 kV. For TEM measurement, the samples were prepared by inserting Cu grids in the GNs powder without using any solvent and by drying the Cu grids with OGNs dispersion casted on. Diffuse reflectance FTIR spectra were recorded via a Cary 630 FTIR spectrophotometer, Agilent Technology, USA, over a range 500–4000 cm^{-1}. X-ray photoelectron spectroscopy (XPS) spectra were collected on a Perkin-Elmer PHI 5400 spectrometer with an Al Kα X-ray source (1486.6 eV) operating at 240 W (12 kV and 20 mA). The spectrometer was calibrated using Au $4f_{7/2}$ at 84.0 eV and Cu $2p_{3/2}$ at 932.7 eV. The base pressure of the analysis chamber was below 10^{-9} mbar. Data analysis was performed using the CasaXPS software package. The room temperature Raman spectra of GNs were obtained on pellets with 10 mm diameter and 2 mm thick and on the dry patch of dispersion of OGNs casted on microscope slide with an iHR550 Raman spectrophotometer, Horiba Jobin–Yvon with a HeNe laser (632.8 nm) as the excitation source.

4 Results and discussion

Figure 1 shows the digital photographs of GNs powder synthesized from the controlled detonation of acetylene with oxygen, the same dispersed in water, and the OGNs dispersed in water with concentrations 1, 0.1 and 0.01 mg/ml. Detonation-produced GNs (Fig. 1a) are a dark, fluffy and light powder. The photographs of dispersions were taken after 11 weeks from the day of a 0.5-h sonication of the GNs and OGNs in water in order to see the stability of the samples' dispersion in water. It can be seen in Fig. 1b that the GNs are not dispersible in water and a small fraction of the GNs used floats on the surface of water, whereas a larger fraction of GNs has settled to the bottom of the vial. OGNs, in contrast to GNs, are dispersible in water as seen in the photograph (Fig. 1c). The color change of the OGNs dispersion, dark black (1 mg/ml) to brown (0.1 mg/ml) to almost clear (0.01 mg/ml), is due to the suspended OGNs sheets with varying concentration. The dispersion shows that the hydrophobic GNs have been transformed to highly hydrophilic OGNs using this approach.

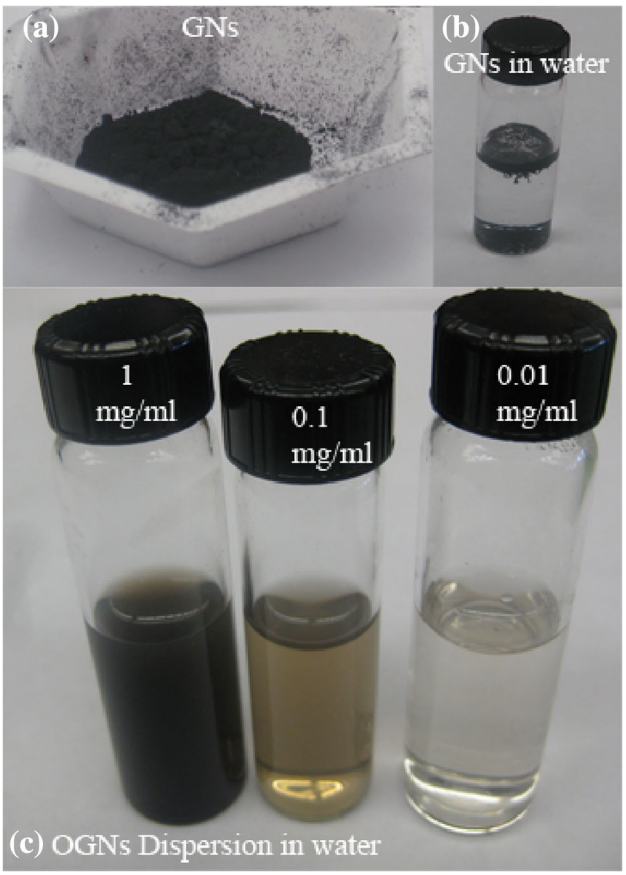

Fig. 1 Images of **a** GNs powder, **b** GNs in water and **c** dispersion of OGNs in water with concentration as marked

The size of the GNs and OGNs sheets is shown in Fig. 2. The GNs are stacked in two to three layers forming the aggregates of nearly circular sheets of size about 225–250 nm [24] as shown in Fig. 2a. Interesting features were observed after the oxidization of these GNs. The stacked GNs transformed into transparent single-layer OGNs with wrinkled ridges (Fig. 2b). The lateral size of the OGNs sheets does not seem to be uniform due to the folding at the edges. However, it can be concluded that the layer morphology of the GNs has been preserved even in OGNs sheets. The size and morphology of GNs and OGNs are further confirmed in supporting information as well by imaging with atomic force microscopy (AFM).

The XRD spectra of the GNs prepared by the detonation of C_2H_2 at $O_2/C_2H_2 = 0.8$ molar ratio and that of OGNs prepared from these GNs are shown in Fig. 3. In Fig. 3a, the most intense and narrow peak on the spectrum of GNs is at $2\theta \sim 26.05°$ corresponding to the (002) planes of stacked graphene layers in GNs [24], whereas that of OGNs is at $2\theta \sim 10.15°$ as shown in Fig. 3b. The nearly featureless region at $2\theta \sim 26.05°$ on the spectrum of OGNs relative to that of GNs indicates that almost all GNs have been oxidized. These XRD spectra indicate that the interplanar spacing (d) of ~0.341 nm for GNs has been shifted to 0.879 nm for OGNs. This increment in the

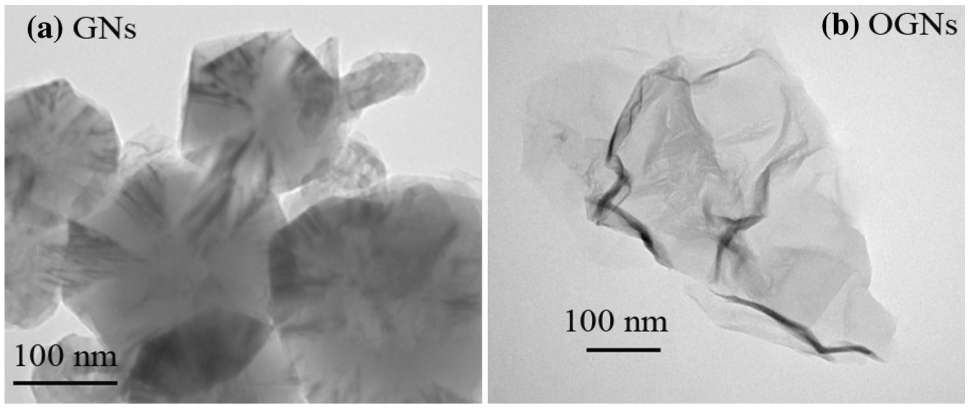

Fig. 2 TEM images of **a** GNs prepared by detonation at $O_2/C_2H_2 = 0.8$ molar ratio [24] and **b** OGNs

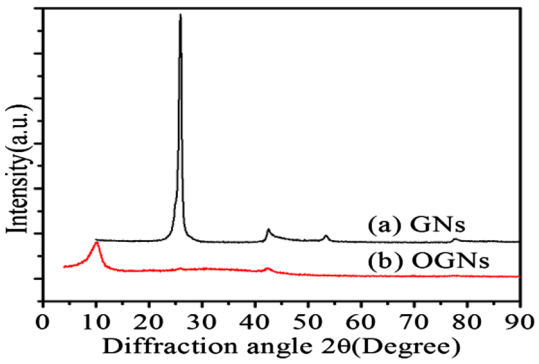

Fig. 3 XRD patterns of **a** GNs prepared by detonation at O_2/C_2H_2 = 0.8 molar ratio [24] and **b** OGNs prepared from GNs

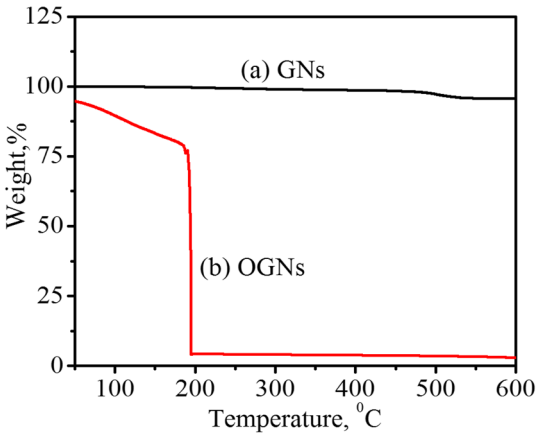

Fig. 4 TGA of **a** GNs and **b** OGNs

interplanar spacing in OGNs is due to the expansion of the layer planes caused by the accommodation of various oxygen species and water molecules while oxidizing GNs [16, 23, 27].

The decomposition characteristics of GNs and OGNs under heat were evaluated by TGA as depicted in Fig. 4. The GNs were observed to be thermally stable with a loss of only ~4 % weight while heated up to 600 °C as shown in Fig. 4a. However, OGNs (Fig. 4b) were thermally unstable with mass lost mainly in two steps: a small fraction, about 25 %, of its weight lost continuously while heating up to 190 °C, and a significant fraction, about 95 %, of its weight lost rapidly at 197 °C. The decreased thermal stability of OGNs is due to the labile oxygen functional groups that yield CO, CO_2 and steam under pyrolysis [20, 28]. Thus, the TGA analysis shows that the GNs were oxidized, and this is consistent with the inference drawn from XRD of GNs and OGNs.

The oxidation of the GNs was further evaluated by Raman spectroscopy. Figure 5 shows the Raman spectra of GNs and OGNs. The three prominent peaks at 1328, 1580

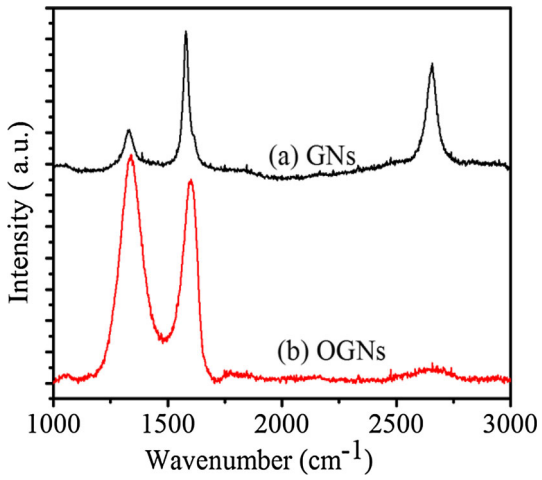

Fig. 5 Raman spectra of **a** GNs prepared by detonation at O_2/C_2H_2 = 0.8 molar ratio [24] and **b** OGNs

and 2650 cm^{-1} on the spectrum of GNs (Fig. 5a) correspond to D-, G- and 2D-bands, respectively. These observed bands are in good agreement with the earlier report [24]. The D-band evolves due to the defect or partially disordered structure of the sp^2 domains in GNs, whereas the G-band is due to the optical E_{2g} phonon at the Brillouin zone center of all sp^2-hybridized carbons in GNs [24, 29]. The 2D-band is the second order of the D-band, sometimes referred to as an overtone of the D-band. Since the 2D-band is the sum of two phonons with opposite momentum, it can be present even if the sample is defects free [30, 31].

The oxidation leads to shifts in the band positions of the D-band and G-band of OGNs (Fig. 5b) by 8 and 20 cm^{-1}, respectively, toward the higher frequency relative to that of GNs. The ratio of the intensity of D-band to intensity of G-band (I_D/I_G ~ 1.13) in OGNs is enhanced four times than that in the GNs (I_D/I_G ~ 0.28). Furthermore, the broadening in FWHM of G-band in OGNs (~90 cm^{-1}) is increased by 1.9 times from that of GNs (~48 cm^{-1}). Moreover, a huge reduction in the I_{2D}/I_G (~0.07) compared to that of GNs (I_{2D}/I_G ~ 0.77) is observed. The blue-shifted and broadened G-band, more intense D-band and less-intense 2D-band in the spectra of OGNs are all consistent with the Raman spectra of graphite oxide reported in the past [32]. Such behavior is due to the disorder-induced reduction in the average size of sp^2 domains by the formation of hydroxyl or epoxies groups with carbon during oxidation of GNs [20, 33, 34] as confirmed by the Drifts-FTIR in Fig. 6.

Figure 6 displays the Drifts-FTIR spectra of GNs and OGNs. The spectrum of GNs (Fig. 6a) is almost featureless and suggests that no functional groups are attached on the surface of GNs and hence they are pristine in nature [24].

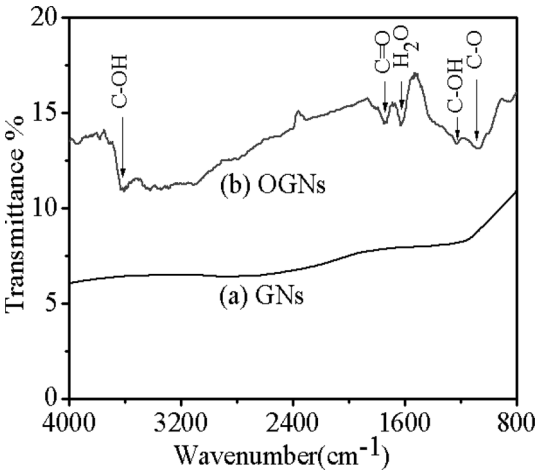

Fig. 6 FTIR of **a** GNs prepared by detonation at $O_2/C_2H_2 = 0.8$ molar ratio [24] and **b** OGNs

However, the Drifts-FTIR spectrum of OGNs (Fig. 6b) has the adsorption bands centered at wave numbers that resemble those mentioned in the previous works [35–39] with the band at $\sim$1073 cm^{-1} attributed to C–O epoxy stretching vibrations, $\sim$1224 cm^{-1} due to C–OH stretching vibrations, $\sim$1623 cm^{-1} from deformation vibration of water molecules, $\sim$1734 cm^{-1} from C=O carbonyl stretching and $\sim$3613 cm^{-1} from stretching vibration of hydroxyl groups. Thus, the GNs have been oxidized extensively, and the surface has been decorated with aforementioned carbonyl, epoxy and hydroxyl functional groups.

More precisely, the surface functional groups present in GNs and OGNs were further explored by X-ray photoelectron spectroscopy (XPS). Two peaks corresponding to the O 1 s and C 1 s are observed in the survey spectrum of GNs in Fig. 7a. The ratio of the carbon to oxygen is estimated to be C/O $\approx$ 49/1, indicating that GNs are very pure. The small peak of O 1 s is probably due to the moisture adsorbed in the system [24]. The survey spectrum of OGNs in Fig. 7b shows a more prominent and intense O 1 s peak relative to that in the survey spectrum of GNs. This indicates that an extensive oxidation of GNs has taken place to yield OGNs. The carbon-to-oxygen (C/O) ratio in OGNs is $\approx$1/1. The C 1 s peak of OGNs was expanded and deconvoluted (Fig. 7c) in order to analyze the other forms of the carbon and oxygen groups. The deconvolution shows the four components of carbon and oxygen groups at around 284.8, 286.4, 287.5 and 288.9 eV which correspond to C=C or C–C, C–O, C=O and O–C=O groups, respectively, as mentioned in the past works [6, 40–43]. Out of the total area under C 1 s peak, 34 % belongs to unoxidized carbon (C=C or C–C), 36 % belongs to carbon attached as epoxy or hydroxyl functional groups (C–O), 22 % belongs to carbonyl (C=O) and the rest of 8 % is the share of carbon attached to carboxylic functional group (O–C=O). The C/O ratio depends on the experimental conditions such as amount of oxidizers, time of reactions and size and morphology of the graphitic material to be oxidized. The C/O ratios that have been achieved so far in graphite oxide sheets after oxidation of graphite using conventional techniques are 2/1 to 4/1 [41, 44]. These C/O ratios are higher than the C/O $\approx$ 1/1 for OGNs prepared here from detonated GNs. Hence, it is worthwhile to highlight that the detonation-produced GNs are unique in the sense that they can be oxidized to a product with the highest level of oxygenation compared to oxides of any other graphitic materials.

Now the question comes across why the detonation-produced GNs get oxidized so heavily. The topic of chemistry and heterogeneity of graphene oxide is still debated [45]. However, what is exciting about graphene is that it can be functionalized on the both faces of a layer, at the edges and at the defects [46]. The surfaces of graphene, in contrast to less-reactive graphite surfaces, are exceptionally reactive [47, 48]. Moreover, the carbon atoms at the graphene edges are more reactive than those at the bulk surface faces [46]. The vacancies, adatoms and point and linear imperfections on the surface enhance the crystal defects in the graphene layers. These defects on the graphene surface are also considered as active sites for chemical reactions [49].

Graphite flakes, the conventional starting material to produce graphene oxide, are a few to several hundred micrometers in size. However, our GNs, the starting material used in this work, are significantly smaller ($\sim$250 nm) than the graphite flakes. Moreover, the specific surface area of GNs ($\sim$25 m^2/g) used here is at least three times more than that of natural graphite (<8 m^2/g). Also, the Raman spectrum of detonation-produced GNs, Fig. 5a, has shown that the GNs have a considerable amount of defects. Thus, detonation-produced GNs have more reactive sites contributed from the boundaries, surfaces and the defects relative to the natural graphite flakes and hence it will be oxidized the most. The type of functional groups and their share for the oxygen content in OGNs have been determined by deconvoluting its XPS O 1 s peak as shown in Fig. 7d. The O 1 s peak of OGNs shows the three components at around 531.7, 532.5 and 533.1 eV which correspond to C=O and O–C=O, C–O and water (H_2O), respectively, as mentioned in the past works [50–52]. The components corresponding to C=O and O–C=O, C–O and H_2O occupy about 30, 40 and 30 % area under O 1 s peak, respectively. Despite significant vagueness regarding the exact location of a particular functional group, it has been reported in the past that most of the carbonyl and carboxyl (C=O and O–C=O) functional groups usually exist at the edges and most of the hydroxyl and epoxy (C–O) groups lie above and below a

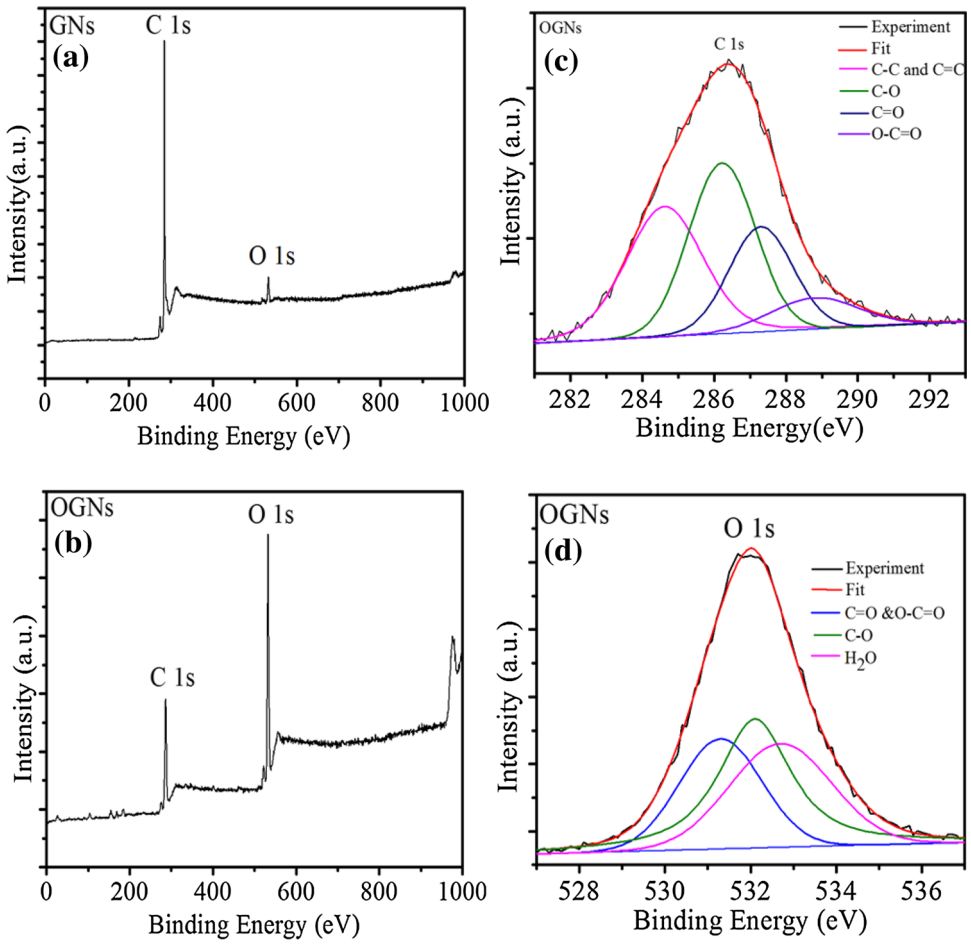

Fig. 7 XPS spectra of **a** GNs prepared by detonation at $O_2/C_2H_2 = 0.8$ molar ratio, survey [24] **b** OGNs, survey **c** C 1 s detail of OGNs and **d** O 1 s detail of OGNs

graphene oxide layer [28, 51, 53]. Thus, we speculate here that out of all O-moieties in OGNs, about 30 % lie on the edges, 40 % lie on the bulk surface of OGNs layer and the rest of 30 % is due to intercalated or chemisorbed water molecules. The oxides attached in this fashion, along with the carbon–carbon chain (C=C or C–C in Fig. 7c) as backbone, still restore the layer morphology of OGNs as shown in TEM image (Fig. 2b).

5 Conclusion

The graphene nanosheets (GNs) produced from the hydrocarbon detonation route have been oxidized. The observed C/O ≈ 1:1 for the oxidized graphene nanosheets (OGNs) is the highest ever level of oxidation of graphitic materials. The OGNs sheets are highly dispersible in water and hence capable of further processing in order to use them for future applications.

Acknowledgments We thank Dr. Daniel L. Boyle, Dr. Leila Maurmann and Dr. Xiuzhi Sun for helping us to obtain TEM images, FTIR and TGA, respectively.

References

1. K.S. Novoselov, A.K. Geim, S.V. Morozov, D. Jiang, Y. Zhang, S.V. Dubonos, I.V. Grigorieva, A.A. Firsov, Science **306**, 666 (2004)
2. G. Wang, J. Yang, J. Park, X. Gou, B. Wang, H. Liu, J. Yao, J. Phys. Chem. C **112**, 8192 (2008)
3. X. Li, X. Wang, L. Zhang, S. Lee, H. Dai, Science **319**, 1229 (2008)
4. P. Blake, P.D. Brimicombe, R.R. Nair, T.J. Booth, D. Jiang, F. Schedin, L.A. Ponomarenko, S.V. Morozov, H.F. Gleeson, E.W. Hill, A.K. Geim, K.S. Novoselov, Nano Lett. **8**, 1704 (2008)
5. G. Wang, X. Shen, B. Wang, J. Yao, J. Park, Carbon **47**, 1359 (2009)
6. D.R. Dreyer, S. Park, C.W. Bielawski, R.S. Ruoff, Chem. Soc. Rev. **39**, 228 (2010)
7. Y.M. Lin, K.A. Jenkins, A. Valdes-Garcia, J.P. Small, D.B. Farmer, P. Avouri, Nano Lett. **9**, 422 (2009)
8. F. Schedin, A.K. Geim, S.V. Morozov, E.W. Hill, P. Blake, M.I. Katsnelson, K.S. Novoselov, Nat. Mater. **6**, 652 (2007)
9. N. Mohanty, V. Berry, Nano Lett. **8**, 4469 (2008)
10. S. Stankovich, D.A. Dikin, G.H.B. Dommett, K.M. Kohlhaas, E.J. Zimney, E.A. Stach, R.D. Pinen, S.T. Nguyen, R.S. Ruoff, Nature **442**, 282 (2006)
11. S. Watcharotone, D.A. Dikin, S. Stankovich, R. Piner, I. Jung, G.H.B. Mommett, G. Evmenenko, S.E. Wu, S.F. Chen, C.P. Liu, Nano Lett. **7**, 1888 (2007)

12. T. Takamura, K. Endo, L. Fu, Y.P. Wu, K.J. Lee, T. Matsumoto, Electrochim. Acta **53**, 1055 (2007)
13. A.K. Geim, K.S. Novoselov, Nat. Mater. **6**, 183 (2007)
14. D. Li, M.B. Muller, S. Gijle, R.B. Kaner, G.G. Wallace, Nat. Nanotechnol. **3**, 101 (2008)
15. C. Shan, H. Yang, D. Han, Q. Zhang, A. Ivaska, L. Niu, Langmuir **25**, 12030 (2009)
16. T. Kuila, S. Bose, A.K. Mishra, P. Khanra, N.H. Kim, J.H. Lee, Prog. Mater. Sci. **57**, 1061 (2012)
17. C. Gómez-Navarro, R.T. Weitz, A.M. Bittner, M. Scolari, A. Mews, M. Burghard, K. Kern, Nano Lett. **7**, 3499 (2007)
18. Y. Xu, H. Bai, G. Lu, C. Li, G. Shi, J. Am. Chem. Soc. **130**, 5856 (2008)
19. H. Becerril, J. Mao, Z. Liu, R.M. Stoltenberg, Z. Bao, Y. Chen, ACS Nano **2**, 463 (2008)
20. S. Stankovich, D.A. Dikin, R.D. Piner, A.K. Kohlhaas, A. Kleinhammes, Y. Jia, Y. Wu, S.T. Nguyen, R.S. Ruoff, Carbon **45**, 1558 (2007)
21. G. Eda, G. Fanchini, M. Chhowalla, Nat. Nanotechnol. **3**, 270 (2008)
22. X. Wang, L. Zhi, K. Mullen, Nano Lett. **8**, 323 (2008)
23. A.D. Dikin, S. Stankovich, E.J. Zimney, R.D. Piner, G.H.B. Dommett, G. Evmenenko, S.T. Nguyen, R.S. Ruoff, Nature **448**, 457 (2007)
24. A. Nepal, G.P. Singh, B.N. Flanders, C.M. Sorensen, Nanotechnology **24**, 245602 (2013)
25. F. Xia, D.B. Farmer, Y.M. Lin, P. Avouris, Nano Lett. **10**, 715 (2010)
26. D.C. Marcano, D.V. Kosynkin, J.M. Berlin, A. Sinitskii, Z. Sun, A. Slesarev, L.B. Alemany, W. Lu, J.M. Tour, ACS Nano **4**, 4806 (2010)
27. T. Szabo, O. Berkesi, P. Forgo, K. Josepovits, Y. Sanakis, D. Petridis, I. Dekany, Chem. Mater. **18**, 2740 (2006)
28. A. Lerf, H. He, M. Forster, J. Klinowski, J. Phys. Chem. B **102**, 4477 (1998)
29. F. Tuinstra, J.L. Koenig, J. Chem. Phys. **53**, 1126 (1970)
30. A.C. Ferrari, J.C. Meyer, V. Scardaci, C. Casiraghi, M. Lazzeri, F. Mauri, S. Piscanec, D. Jiang, K.S. Novoselov, S. Roth, A.K. Geim, Phys. Rev. Lett. **97**, 187401 (2006)
31. D.C. Elias, R.R. Nair, T.M.G. Mohiuddin, S.V. Morozov, P. Blake, M.P. Halsall, A.C. Ferrari, D.W. Boukhvalov, M.I. Katsnelson, A.K. Geim, K.S. Novoselov, Science **323**, 610 (2009)
32. K.N. Kudin, B. Ozbas, H.C. Schniepp, R.K. Prud'homme, I.A. Aksay, R. Car, Nano Lett. **8**, 36 (2008)
33. T.C. Chieu, M.S. Dresselhaus, M. Endo, Phys. Rev. B **26**, 5867 (1982)
34. A.A. Alhwaige, T. Agag, H. Ishida, S. Qutubuddin, RSC Adv. **3**, 16011 (2013)
35. S. Stankovich, R.D. Piner, S.T. Nguyen, R.S. Ruoff, Carbon **44**, 3342 (2006)
36. T. Szabo, O. Berkesi, I. Dekany, Carbon **43**, 3181 (2005)
37. G.I. Titelman, V. Gelman, S. Bron, R.L. Khalfin, Y. Cohen, H. Bianco-Peled, Carbon **43**, 641 (2005)
38. H. Zhang, D. Hines, D.L. Akins, Dalton Trans. **43**, 2670 (2014)
39. G.P. Singh, K.M. Shrestha, A. Nepal, K.J. Klabunde, C.M. Sorensen, Nanotechnology **25**, 265701 (2014)
40. J. Shang, L. Ma, J. Li, W. Ai, T. Yu, G.G. Gurzadyan, Sci. Rep. **2**, 792 (2012)
41. G. Eda, M. Chhowalla, Adv. Mater. **22**, 2392 (2010)
42. J.I. Paredes, S. Villar-Rodil, A. Martinez-Alonso, J.M.D. Tascon, Langmuir **24**, 10560 (2008)
43. A. Kolmakov, D.A. Dikin, L.J. Cote, J. Huang, M.K. Abyaneh, M. Amati, L. Gregoratti, S. Gunther, M. Kiskinova, Nat. Nanotechnol. **6**, 651 (2011)
44. W.S. Hummers, R.E. Offeman, J. Am. Chem. Soc. **80**, 1339 (1958)
45. V. Georgakilas, M. Otyepka, A.B. Bourlinos, V. Chandra, N. Kim, K.C. Kemp, P. Hobza, R. Zboril, K.S. Kim, Chem. Rev. **112**, 6156 (2012)
46. M. Quintana, J.I. Tapia, M. Prato, Beilstein J. Nanotechnol. **5**, 2328 (2014)
47. R. Sharma, J.H. Baik, C.J. Perera, M.S. Strano, Nano Lett. **10**, 398 (2010)
48. M. Quintana, K. Spyrou, M. Grzelczak, W.R. Browne, P. Rudolf, M. Prato, ACS Nano **4**, 3527 (2010)
49. F. Banhart, J. Kotakoski, A.V. Krasheninnikov, ACS Nano **5**, 26–41 (2011)
50. O. Akhavan, Carbon **48**, 509 (2010)
51. A. Ganguly, S. Sharma, P. Papakonstantinou, J. Hamilton, J. Phys. Chem. C **115**, 17009 (2011)
52. K. Haubner, J. Murawski, P. Olk, L.M. Eng, C. Ziegler, B. Adolphi, E. Jaehne, ChemPhysChem **11**, 2131 (2010)
53. D. Hadzi, A. Novak, Trans. Faraday Soc. **51**, 1614 (1955)